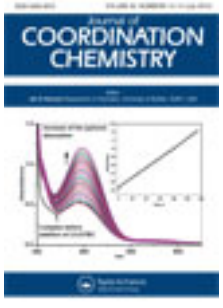

Journal of Coordination Chemistry
Publication details, including instructions for authors and subscription information:
http://www.tandfonline.com/loi/gcoo20

Review of the synthesis and properties of colloidal quantum dots: the evolving role of coordinating surface ligands

Christopher M. Evans [a], Laura C. Cass [a], Kathryn E. Knowles [a], Daniel B. Tice [a], Robert P.H. Chang [b] & Emily A. Weiss [a]

[a] Department of Chemistry, Northwestern University, 2145 Sheridan Rd., Evanston, IL 60208, USA

[b] Department of Materials Science and Engineering, Northwestern University, 2220 Campus Drive, Evanston, IL 60208, USA

Accepted author version posted online: 17 May 2012.Published online: 06 Jun 2012.

To cite this article: Christopher M. Evans, Laura C. Cass, Kathryn E. Knowles, Daniel B. Tice, Robert P.H. Chang & Emily A. Weiss (2012) Review of the synthesis and properties of colloidal quantum dots: the evolving role of coordinating surface ligands, Journal of Coordination Chemistry, 65:13, 2391-2414, DOI: 10.1080/00958972.2012.695019

To link to this article: http://dx.doi.org/10.1080/00958972.2012.695019

Journal of Coordination Chemistry
Vol. 65, No. 13, 10 July 2012, 2391–2414

Review of the synthesis and properties of colloidal quantum dots: the evolving role of coordinating surface ligands

CHRISTOPHER M. EVANS†, LAURA C. CASS†, KATHRYN E. KNOWLES†, DANIEL B. TICE†, ROBERT P.H. CHANG‡ and EMILY A. WEISS*†

†Department of Chemistry, Northwestern University, 2145 Sheridan Rd., Evanston, IL 60208, USA
‡Department of Materials Science and Engineering, Northwestern University, 2220 Campus Drive, Evanston, IL 60208, USA

(*Received 8 May 2012; in final form 28 May 2012*)

This review highlights the developments in synthetic methods for colloidal quantum dots that have expanded the range of achievable sizes, shapes, materials, and surface chemistries over the past 30 years, and how these methods have enabled optimization of properties like photoluminescence quantum yield, monodisperse size distributions, and conductivity in the solid state.

Keywords: Quantum dot; Photoluminescence; Metal chalcogenide; Passivation

1. Introduction

This review describes the evolution of the role of coordinating ligands in the synthesis of colloidal semiconductor quantum dots (QDs), crystalline structures, the sizes of which are in the order of the Bohr-exciton radius for the bulk semiconductor material [1], and the influence of these ligands on the structural, optical, and electronic properties of the resulting QD-ligand complexes. We highlight developments in the use of coordinating ligands in the QD synthesis from the past 30 years that have expanded the range of achievable sizes, shapes, materials, and surface chemistries. This synthetic versatility enables exploration of a vast parameter space that allows optimization of properties, such as photoluminescence (PL), quantum yield (QY), size dispersion, and solid-state conductivity, that make QD materials suitable for a range of applications from biological imaging to photovoltaics.

*Corresponding author. Email: e-weiss@northwestern.edu

ISSN 0095-8972 print/ISSN 1029-0389 online
http://dx.doi.org/10.1080/00958972.2012.695019

2. Arrested precipitation

2.1. *Arrested precipitation methods produced the first soluble semiconductor colloids*

The earliest report of the formation of nanoscale semiconductors was in 1981 and focused on their photolytic cleavage of H_2O [2]. Prior work using bulk semiconductors such as CdS and GaP demonstrated the ability of these systems to oxidize water at significantly more negative potentials than the standard redox potential of the H_2O/O_2 couple [3, 4]; however, photo-degradation pathways limited the effectiveness of these model systems. Gratzel *et al.* [2] developed microelectrodes comprising ''colloidal CdS'' that ''exhibited surprisingly high activity as a water-cleaving catalyst'' when loaded with active catalysts (Pt, RuO_2) and irradiated with visible light. The efficacy of these semiconductor photoelectrochemical cells for solar energy conversion [5] inspired the field of dye-sensitized solar cells [6], and the aqueous arrested precipitation synthesis developed by Gratzel in this work became the standard method of semiconductor nanoparticle (QD) formation for many years.

The arrested precipitation method is based on the low solubility product (K_{sp}) of binary semiconductor alloys in aqueous solutions [7]. For instance, the K_{sp} values for II–VI semiconductor sulfides ZnS, CdS, and HgS in water are 2×10^{-25}, 8×10^{-28}, and 2×10^{-53}, respectively. There exists, therefore, a large driving force to produce precipitates once the cation and anion pairs are in sufficient concentrations to reach super-saturation. An aqueous solution containing a combination of metal salt precursors, such as $Cd(SO_4)_2$ and $(NH_4)_2S$, establishes a dynamic equilibrium (equation 1) that favors the precipitation of solid CdS due to its extremely low K_{sp} value. In practice, Gratzel's method involves the slow injection of an aqueous solution of $Cd(SO_4)_2$ into an alkaline solution (pH 10) containing maleic anhydride/styrene copolymer and $(NH_4)_2S$. The presumed role of the copolymer is to stabilize the colloidal dispersions of CdS and prevent the formation of aggregates and subsequent precipitation; however, there is little discussion in Gratzel's and other early work that used polymeric additives to explain unusual stability of the colloidal dispersions of CdS.

$$Cd^{2+}_{(aq)} + S^{2-}_{(aq)} \leftrightarrow CdS_{(s)} \tag{1}$$

The formation of colloidal dispersions of CdS is evidenced by the development of a bright-yellow color. The absorption spectrum of a solution containing CdS colloids made *via* Gratzel's arrested precipitation procedure is relatively featureless, but has a shoulder at 520 nm, consistent with the bandgap of bulk CdS. These colloids do not exhibit the higher-energy absorption features indicative of quantum confinement, but the early arrested precipitation syntheses still had value as a cheaper and safer solution-phase alternative to solid-state approaches for the production of bulk semiconductors, such as molecular beam epitaxy and metal-organic chemical vapor deposition [8, 9].

2.2. *The discovery of quantum size effects, and initial efforts to decrease size dispersity*

In the first reports of nanocrystalline semiconductors, researchers relied on a combination of techniques to determine the size distribution of their particles. Henglein used filtration through pores of known size to determine upper bounds for the diameters of colloidal CdS [10–13], while Gratzel [2] and Brus [14] used light

scattering to determine hydrodynamic radii. These techniques, however, are significantly limited in their accuracy and ability to address the shape anisotropy of particles, so the application of transmission electron microscopy (TEM) to these systems greatly improved the accuracy of size and shape measurements. Brus and co-workers [15] first used TEM to image colloidal CdS, which lead to the first observation of size-dependent optical properties for semiconductor colloids. The authors showed that the absorption spectrum for CdS nanocrystals with diameters of 4.5 nm was strongly blue-shifted from the bulk band-edge (by ~200 meV), while larger nanocrystals (12.5 nm diameter, produced by aging fresh colloids for 1 day at pH 3) had an absorption spectrum consistent with the bandgap of the bulk material. This discovery represented the first demonstration of quantum confinement in a solution-phase sample. Previous work on quantum wells had shown a measurable size-dependence (i.e. quantum confinement) in 1-D thin layers of GaAs grown by molecular beam epitaxy [16, 17]; however, this technique is expensive and, at the time, had limited control over thickness. Brus' discovery of the correlation between bandgap energy, as measured by absorption spectroscopy, and size in colloidal semiconductors provided a model system for studying quantum confinement that was much cheaper and easier to synthesize than quantum wells. Further, it showed that confinement in all 3-D amplified the sensitivity of the optical spectra to particle size.

Simple calculations based upon a particle-in-a-box model system adequately described size-effects in colloidal QDs for all but the smallest sizes [18]. Experimental control of the nanocrystal size was inconsistent, however, mostly because it was achievable only by day-long aging of fresh colloids in acidic conditions [7, 15]. The solubility of metal sulfides is higher at low pH values, therefore acidic conditions slow nucleation from super-saturation and facilitate the growth from ions still in the solution. Unfortunately, higher solubility also favors the reverse reaction (equation (1)) that dissolves nucleated CdS and promotes Ostwald ripening; this type of growth broadens size distributions and obscures the observation of discrete optical transitions. If acetonitrile is used as the solvent for arrested precipitation instead of water, the resulting diameter of CdS nanocrystals is much smaller, probably due to faster nucleation kinetics (the solubility product of the metal sulfides is even smaller in organic solvent than in water). Further support for this hypothesis can be drawn from the growth of ZnS in methanol [19]. ZnS colloids were produced by adding Na_2S to $Zn(ClO_4)_2$ in both methanol and water solutions. As shown in figure 1, the absorption peaks are narrower and positioned at higher energy for particles synthesized in methanol than for particles synthesized in water. This result implies that the ZnS particles made in methanol are smaller and have a tighter size distribution than their aqueous analogs. As was the case for acetonitrile, the poor solubility of metal sulfides in methanol results in rapid and uniform nucleation kinetics, and a small and narrow diameter distribution.

2.3. *The role of stabilizers in QDs formed by arrested precipitation*

Within the arrested precipitation mechanism, the optical spectra of synthesized ZnS colloids are fairly insensitive to the Zn^{+2} source (it was varied from nitrate to perchlorate, tetrafluoroborate, bromide, and chloride) – that is, the coordinative environment of the reagent salts; however, polymer additives were necessary to inhibit

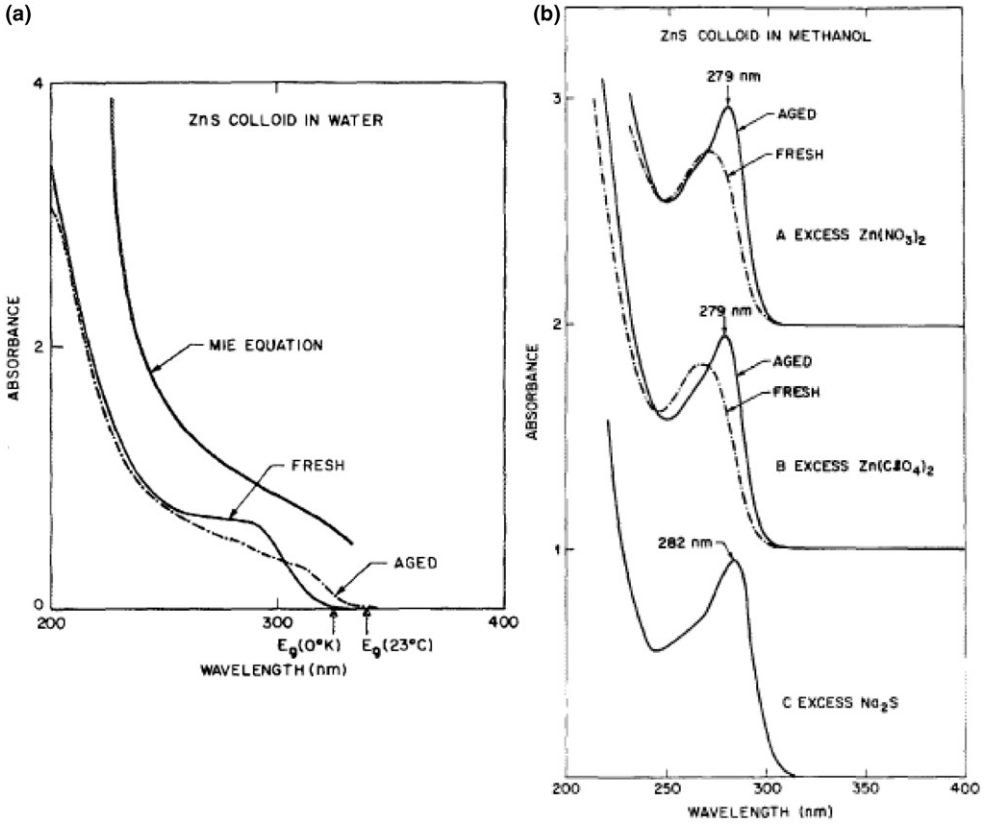

Figure 1. ZnS produced by arrested precipitation in (a) water and (b) methanol. Reactions in methanol yield narrower size distributions and smaller sizes than reactions in water while also inhibiting Ostwald ripening during aging. Reprinted with permission from [19]. Copyright 1985, American Institute of Physics.

rapid precipitation. Without these stabilizers, such as maleic anhydride/styrene copolymer [2, 7, 14, 15], SiO_2-sol [10–12], metal sulfides would simply precipitate from the aqueous solution [7]. Very little detail was provided in these papers regarding the exact role of styrene copolymer. Likely, upon exposure to water, the maleic anhydride units in the copolymer undergo hydrolysis and generate numerous carboxylic acid groups along the alternating polymer backbone. Carboxylic acids represent a good functional group for cation ligation; therefore, it is possible that, upon hydrolysis, the copolymer chelates both surface cation sites and free Cd^{2+} ions in the solution. This mechanism might explain the exceptional stability of CdS in aqueous solutions in the presence of copolymer. Similarly, SiO_2-sol was proposed to stabilize nanocrystals by promoting the adsorption of Zn^{2+} cations and providing nucleation centers for the reaction with sulfide anions (figure 2) [13]. Many different stabilizers have now been utilized in arrested precipitation: glycerol [20], $(NaPO_3)_6$ [20, 21], polyethylene glycol [22], polyvinyl acetate [20], and polyvinyl alcohol [23]. These systems have not been studied rigorously, but it is reasonable that they contribute to either metal chelation or emulsion formation to stabilize nanocrystals.

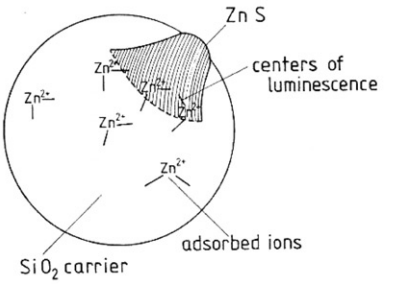

Figure 2. SiO_2 sol serves as a nucleation center for formation of ZnS nanocrystals. Reprinted with permission from [13]. Copyright 1984, Wiley.

2.4. *Issues with QDs formed by arrested precipitation*

By 1985, a host of different binary semiconductors (ZnS, ZnSe, CdS, and PbS) were synthesized by arrested precipitation under mild conditions (aqueous solvent and room temperature), but, in samples of nanocrystals produced by this method, the PL was very weak and energetically broad. PL represents a relative measure of the e^- and h^+ populations and their temporal/spatial overlap within the nanocrystal. Therefore, PL is very sensitive to factors that alter the populations of excited-state carriers, such as surface processes. For instance, photocorrosion (equation (2)) is a well-known process in bulk semiconductors whereby photo-generated holes diffuse to the surface and "dissolve" the lattice [5]. This process should be enhanced in nanoscale systems where the surface represents a much larger contribution of the total volume. Besides corrosion, this process also quenches luminescence by providing a non-radiative relaxation pathway for hot carriers. The low PL-QYs in nanocrystals produced by arrested precipitation imply that non-radiative processes dominate charge recombination, and the large emission Stokes shifts (~400 meV) and long radiative lifetimes (~μs) suggest localized charge-trapping at surface defects.

$$2h^+ + CdS \rightarrow Cd^{2+} + S \tag{2}$$

Another issue with the arrested precipitation method was that controlling the size of the nanocrystals using this method remained challenging. The only means of size-control were kinetically controlling reactivity at different temperatures [12, 19] or nanocrystal "aging" [7, 15, 20]. As was discussed previously, aging in acidic solutions merely induces Ostwald ripening, which is deleterious to size distributions. Reactions at −77°C produced smaller ZnS than at 25°C, but diameters of the resulting nanocrystals only changed from 1.0 nm for those synthesized at −77°C to 1.9 nm for those synthesized at 25°C. Synthetic improvements to the arrested precipitation method eventually allowed for narrower size distributions [24], which enabled the observation and investigation of higher-order optical transitions and vibronic effects that were not resolvable in more polydisperse samples [25]. Further achievements in nanoscale photophysics and device applications, however, would require researchers to develop methods other than arrested precipitation to synthesize high-quality nanocrystals.

3. Templated growth

3.1. *Nanocrystal growth in micelles*

For many years micelles and related structures (such as lipid vesicles and membranes) have been used as convenient hosts for the building blocks of macromolecular structures [26]. These techniques have been applied for the preparation and characterization of many different monodisperse particles, including biomolecules [27], magnetic materials (magnetite, ferro fluids) [28, 29], and metals (Ag, Pt, Pd, Ir, Rh) [30]. In fact, the use of micellular methodologies for producing gold nanostructures has been known since Faraday's time [31, 32]. The enabling feature of inverse micelles is the synthetic control over the size of the interior volume of the micelle. The volume can be tuned by varying the ratio of [H_2O] to [surfactant] (ω); in general, increasing this ratio will increase the volume of a micelle's interior. This interior serves as a microreactor that controls the concentration of ionic reagents, and confines reactions to a particular volume. Spatial confinement within micelles, bilayers, or vesicles precludes the particle growth by either Ostwald ripening or agglomeration [26].

Growth of semiconductor particles within micelles was first attempted by Fendler and co-workers [33], who successfully produced CdS within AOT (sodium di-2-ethylhexyl sulfosuccinate)-inverted micelles. The AOT-inverted micelles in iso-octane contained $CdCl_2$ and $(NaPO_3)_6$ and were then exposed to controlled amounts of H_2S to produce CdS at room temperature. Based on light scattering, the diameter of the inverted micelle only slightly increased after the reaction (12 nm to 15 nm), which indicated that the micelles were not perturbed or destabilized during the reaction. Furthermore, TEM images of CdS particles produced with this reaction (diameter ~10 nm) closely matched the predicted size of the micelle interior. Further studies were undertaken to exploit the potential of inverted micelles as macromolecular templates to control nanoparticle size, shape, and stability [23, 34]. As shown in figure 3(a), the size

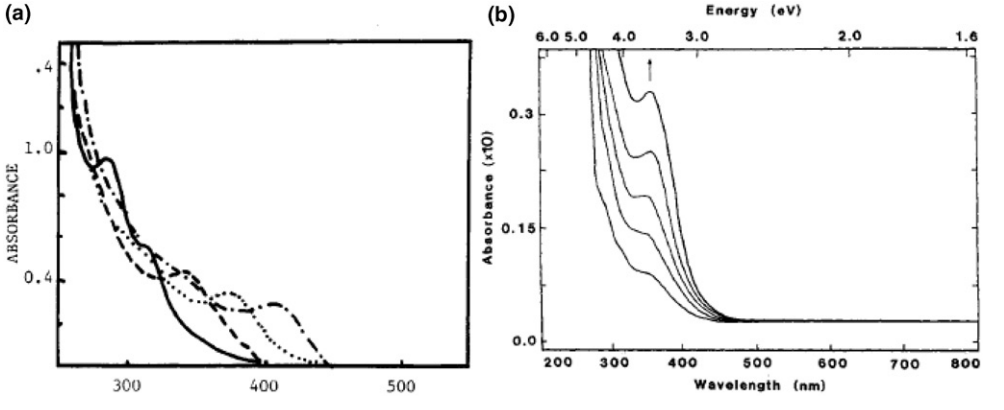

Figure 3. (a) Absorption spectra of CdS grown in reverse micelles as a function of the water/surfactant ratio, ω (solid line $\omega = 1.0$, dashed line $\omega = 2.8$, dotted line $\omega = 4.7$ and dash-dot line $\omega = 8.4$). The CdS diameter is proportional to ω. Reprinted with permission from [23]. Copyright 1986 American Chemical Society. (b) Time-dependent changes in absorption spectra of CdS grown within a vesicle. The increase in optical density without any spectral shifting indicates that CdS growth occurs within vesicles and that nanoparticle size is constrained. Reprinted with permission from [35]. Copyright 1987 American Chemical Society.

of CdS increases proportionally with the size of the interior. The CdS diameter could be tuned between 1.3 and 4.1 nm, a feat not possible using prior techniques [23]. These studies also demonstrated that the protective environment of the micelle inhibits particle growth by Ostwald ripening and produces particles that are stable indefinitely, unlike those made from arrested precipitation in water.

The slow growth kinetics for reactions produced within an inverse micelle afford the potential to monitor directly the formation of CdS nanocrystals [35]. Figure 3(b) shows optical absorption spectra taken at regular intervals during the reaction; the slow growth of CdS is evidenced by the monotonic increase in the optical density without significant shift in energy.

The considerable success using micelles as templates motivated the use of several other template systems such as zeolites [36], polypeptide cages [37], and living cells [38–41]. Biomimetic synthesis of nanostructures has been successfully used to produce magnetite, silica [40], and silver nanoparticles [39, 41]. CdS nanocrystals were grown from two different yeast strains (*Candida glabrata* and *Schizosaccharomyces pombe*) cultured in the presence of cadmium salts [38]. These particles display narrow absorptions comparable to the best chemically produced nanocrystals and are even crystalline (based on X-ray diffraction and TEM). Each yeast strain yielded monodisperse CdS of different sizes suggesting that the wide variability in shape and size for single-cell organisms could be exploited to control nanoscale morphology. Polypeptide cages have also been shown to produce CdS by exposing apoferritin to an aqueous cadmium acetate solution followed by the addition of Na_2S [37]; however, diameters of CdS particles made with this method are not consistent with the size of the interior cage. This discrepancy is likely due to independent nucleation events occurring inside and outside of the apoferritin cage since binding sites exist both on the interior and exterior of the cage. Zeolites have been used as a synthetic template as well but, as with polypeptide cages, nanocrystal growth was not confined within the zeolite pores; diameters were shown to be widely variable and independent of pore size [36].

In summary, templated growth of semiconductors was widely adopted and capable of producing large varieties of semiconductors: CdS [23, 33–35, 38], CdSe [42], CdTe [42], Cd_3As_2 [23], ZnS [43], ZnSe [44], PbS [36], HgS [45, 46], and HgSe [42] with significant improvements in size-control. Yet, the nanocrystals' photophysics was still dominated by inhomogeneous broadening. Transient photophysical hole burning measurements confirmed that typical samples had absorption linewidths (for the lowest allowed optical transition) seven times broader than the intrinsic homogeneous widths ($140\,cm^{-1}$) [47]. Nonetheless, template methods yielded significant improvements in size-dispersity compared with arrested precipitation methods. This improvement allowed for many fundamental photophysical and structural characterizations, which helped to elucidate the structure and optical properties of nanocrystals [44, 48–50].

3.2. *The emergence of the role of surface chemistry in PL*

The PL spectra of nanocrystals produced from early arrested precipitation and template methods were typically broad and weak. Due to their nanoscale dimension, surface atoms represent a very large fraction of the total number of atoms within a single nanocrystal. Each surface site represents a structural defect and a possible site for charge-trapping. Henglein and coworkers were the first to investigate the influence of

surface chemistry on the PL properties of semiconductor colloids. They found that CdS colloids, which were made *via* arrested precipitation in the presence of a silica sol, exhibited a PL peak that was broad, long-lived (~1 μs) [51], and dramatically Stokes-shifted (380 meV) from the band-edge. The PL-QY of this emission was very sensitive to the presence of excess cations and anions in the solution [11]. A host of anions (S^{2-}, Br^-, I^-, CLO_4^-, Cl^-, SO_4^{2-}, NO_3^-, SCN^-, and F^-, in the order of decreasing efficiency) served as effective quenchers of the PL, while excess $Cd(ClO_4)_2$ enhanced the PL (figure 4). The authors proposed that the anions scavenged excited-state charges at the surface of CdS, but they had, at the time, no adequate explanation for the beneficial effect of cations.

The cation enhancement effect was also observed later in 1982 by Rossetti and Brus; they saw increase in PL intensity of as much as 35% when CdS was exposed to Zn^{2+} ions [14]. The authors' explanation of this result represents an important advancement in our understanding of the nature of the surfaces of QDs; the authors stated that "the role of Zn^{2+} is not to provide impurity atom radiative recombination centers," but to slow the nonradiative recombination by passivating surface sites that would otherwise trap the hole. Numerous subsequent experiments supported this explanation, and it motivated the development of core/shell nanoparticles, which consist of nanocrystal cores coated with a wider bandgap semiconductor to coordinatively passivate defect sites, improve electron–hole overlap, and therefore improve radiative electron–hole recombination [43, 52, 53]. Bawendi and co-workers made the first core/shell QDs by exposing CdSe nanocrystals, stabilized within AOT inverted micelles, to 20 alternating injections of $Zn(ClO_4)_2$ and thiophenol to build-up a ZnS shell epitaxially onto the seed nanocrystals [43]. As a consequence, the previously broad deep-trap emission was replaced with band-edge emission and the PL-QY of core/shell nanocrystals (CdSe/ZnS) increased by a factor of 10 when compared to the seed nanocrystals.

An alternative means of producing heterostructure core/shell structures to both passivate surface defects and for the generation of novel quantum structures (e.g., quantum wells) utilizes the concept of cation exchange [45]. Weller and co-workers added Hg^{2+} salts to CdS seeds, which resulted in a substitution reaction (equation (3)) driven by the dramatic difference between the solubility products of HgS and CdS (K_{sp} for HgS is ~26 orders of magnitude smaller than CdS). Inductively coupled plasma

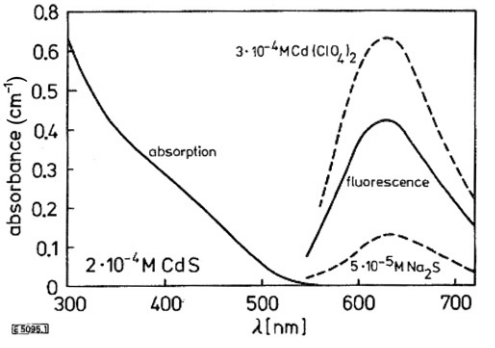

Figure 4. The fluorescence spectrum for CdS nanocrystals is sensitive to certain additives: cation sources enhance the emission while anionic sources quench CdS emission. Reprinted with permission from [11]. Copyright 1982, Wiley.

mass spectroscopy (ICP-MS) and polarography proved that these reactions are quantitative (i.e., every Hg atom gets incorporated into the nanocrystal lattice by replacing a Cd atom). By carefully controlling Hg^{+2} stoichiometry, the thickness of HgS shell can be systematically controlled [46].

$$(CdS)_m + nHg^{2+} \rightarrow (CdS)_{m-n}(HgS)_n + nCd^{2+} \quad (3)$$

The first paper to introduce ligand exchange as a method of PL enhancement showed that the addition of tertiary amines (NEt_3, NMe_3, DABCO) to CdS and Cd_3As_2 QDs increased the PL-QY by up to 450% and converted deep-trap emission to band-edge emission [23]. Interestingly, aromatic amine (pyridine) did not enhance emission. This effect suggests that it is not simply chemical passivation of the surface that leads to changes in PL, but rather electronic interactions between the ligand and the QD [54]. In these examples of PL enhancement, surface treatment fills deep-trap states and allows radiative recombination from band-edge states, which have nanosecond lifetimes as opposed to the microsecond lifetimes associated with defect emission [55]. Rossetti *et al.* also observed that the PL intensity of solutions containing CdS colloids increased (and switched from deep-trap to band-edge emission) when they decreased the pH to 3 from basic conditions [15]. Adsorbed S^{2-} ions at pH 3 become SH^- and are thus less prone to reduction by the excited state of the QD, which is a common quenching mechanism for QDs [14]. For example, benzoquinone [14] and methylviologen [10] are both good electron acceptors and both quench the PL of CdS QDs. Charge transfer from nanocrystal surfaces to adsorbed surface ligands (e.g., S^{2-}) and electron acceptors in solution was clearly efficient; more importantly at the time, however, these results began to elucidate the importance of surface structure in the optical properties of nanoscale systems.

4. Organometallic synthesis

4.1. *The development of organometallic precursors*

Hydrogen chalcogenide precursors (H_2Ch, Ch=S, Se, Te) were used successfully in the arrested precipitation method [13, 20, 25]. While some authors still used ionic sulfur sources [34] (e.g., Na_2S) the hydrogen chalcogenide precursors typically produced more homogeneous size distributions. The trend toward organometallic reagents quickened with the utilization of bis(trimethylsilyl)selenide as an anion source [42]. Reagents of the form (bis(TMS)Ch) have been used prior for the preparation of many bulk semiconductors [56–59] and some have suggested that they can be envisioned as ''organometallic equivalents of chalcogenide dianions'' [42]. Steigerwald *et al.* first used this reagent for the production of HgSe and CdSe within AOT inverse micelles [42]. As said before, the nanocrystal size was tunable based on ω, but, more importantly, they also reported that additional injections of reagents resulted in the growth of larger particles, rather than inducing independent nucleation events. Growth occurs analogously to monomer addition whereby single atoms of Cd (or Ch) react with exposed surfaces at the interface. Based on these observations, these authors characterized colloidal crystallites as ''inorganic living polymers'' which are stable in the solution but capable of interfacial reaction with monomers in solution. This is a

noteworthy classification for nanocrystals as it considers that their inherent crystal structure produces a polymer-like core composed of repeating units. Furthermore, surface derivation of nanocrystals with silylorganoselenides (e.g., $PhSeSiMe_3$) demonstrated that Cd-rich surfaces undergo surface termination when exposed to a reactive chalcogenide precursor (figure 5). The nanocrystal grows slightly, but most remarkably this process alters the surface chemistry from hydrophilic to hydrophobic, which makes the nanocrystals soluble in organic solvents such as DMF, DMSO, toluene, and pyridine rather than water.

4.2. *The emergence of tertiary phosphines as the anionic precursor for QDs*

The successful replacement of ionic anion sources with H_2Ch and bis(TMS)Ch motivated many researchers to further examine organometallic precursors for nanocrystal synthesis. For semiconductors produced by organometallic vapor-phase epitaxy (OMVPE), organometallic reagents were already commonplace and typically employed metal alkyl compounds (e.g. $CdMe_2$, $TeEt_2$) [60]. However, high reaction temperatures ($>200^{\circ}C$) were generally necessary for pyrolysis of the very stable alkyl chalcogenides. Alternatively, tertiary phosphine chalcogenides (R_3PCh) have been described as single-coordinate complexes of Ch^0 [61]. They are known to be significantly less stable than their alkyl analogs; Et_3PTe decomposes upon gentle heating yielding Te metal [62]. Additionally, R_3PTe was shown to decompose in galvanic cells, when combined with Cd-salts, to produce CdTe thin-films [63]. Steigerwald *et al.* were the first to utilize tertiary phosphine chalcogenides for the solution-phase synthesis of semiconductors [64]. These authors achieved quantitative yields of HgTe powder when stirring Et_3PTe with Hg metal in toluene for 20 h. Motivated by the abundant use of metal alkyls for OMVPE, the authors attempted using $HgEt_2$ but found it to be less reactive and required significant heating. Even so, conversion yields after 24 h of heating were lower for the Hg-alkyls (70%) than for Hg-metal (99% at R.T.); although, yields could be improved to 95% by changing the Hg-alkyl substituent from ethyl to phenyl. Metal-alkyl complexes have also been used with bis(TMS)Ch anion sources with success, though the yields were lower and reaction temperatures were much higher ($400^{\circ}C$) [65].

Proven successful for HgTe, R_3PCh would be later used for the production of NiTe [66], MnTe [67], FeTe [68], PdTe [69], CoTe [70], CoSe [71], and CoS [71]. In each case, combinations of homoleptic zero-valent metal cation sources (e.g., $Ni(COD)_2$,

Figure 5. Generalized schematic for the ligand exchange of AOT encapsulated CdSe (left) for alkyl groups (e.g. R). Reprinted with permission from [42]. Copyright 1988 American Chemical Society.

$Pd(PPh_3)_4$, $Co_2(CO)_8$) and tertiary phosphine chalcogenides produced novel cluster compounds. Likely, the instability of R_3PTe leads to rapid depletion of precursor during nucleation, leaving little reagent available for subsequent growth. In all the semiconductors produced from tertiary phosphine chalcogenides that are listed above, the synthesis exclusively yields cluster compounds. For instance, $Ni_9Te_6(PEt_3)_8$ and $Ni_{20}Te_{18}(PEt_3)_{12}$ (figure 6) are produced by controllably varying reagent stoichiometry [66]. These species represent molecular-like reaction intermediates that mimic the structure of their respective solid-state crystals, just much smaller. With respect to PdTe, it was concluded that the bulk PdTe crystal can be interpreted as a very organized polymer of the Pd_2Te_2 rhombus; which well matches the identity of the cluster product [69]. Further reinforcing the relationship between cluster and crystalline semiconductor, thermolysis of each cluster compound lead to the formation of bulk semiconductor, but at much lower temperatures than those required with elemental sources [69].

Cluster intermediates are also observed in reactions between tertiary phosphine chalcogenides and non zero-valent metal sources (e.g., metal alkyls). In these instances, $M(ChR)_2$ compounds are produced by chalcogenide insertion in between M–C bonds. Pyrolysis of $Hg(TeR)_2$ crystals, in vacuum at 120°C, produced HgTe [72] and this methodology has been shown to be general [73] for most of the II–VI semiconductors. While pyrolysis is capable of producing a variety of semiconductors from molecular sources, the size of the resulting particles are very large and rarely is quantum confinement ever observed. Temperature-programmed desorption mass spectrometry demonstrated that a nanocrystal's ligands desorb at temperatures commonly used for pyrolysis, leaving no steric barrier for interparticle fusion [50].

It was observed that sizes determined from XRD spectra, for pre-annealed nanocrystals, were inconsistent with diameters obtained by TEM [74]. Where volatile ligands (e.g., PMe_3, TMS) desorb, a procedure was developed whereby nanocrystal seeds, produced from inverted AOT micelles, could be annealed at 200°C in a melt composed of 90% tributylphosphine (TBP) and 10% TBP oxide (both compounds have

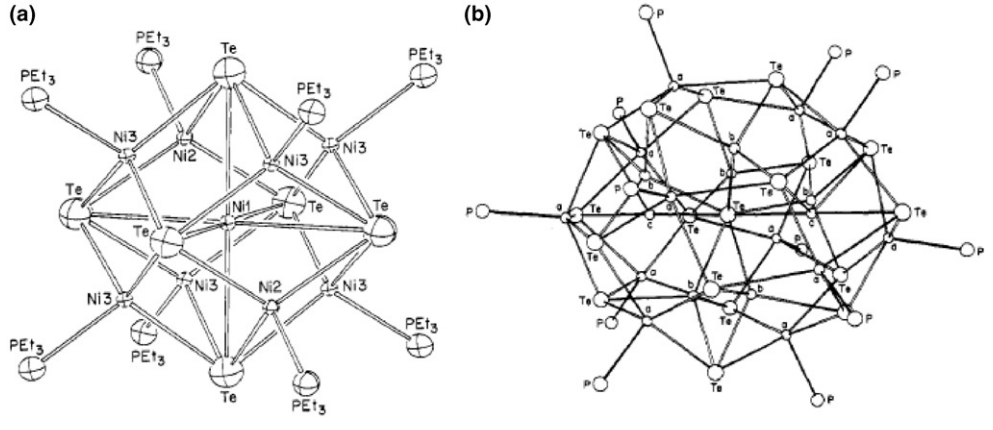

Figure 6. Molecular cluster intermediates produced from the reaction between $Ni(COD)_2$ and Et_3PTe: (a) $Ni_9Te_6(PEt_3)_8$ and (b) $Ni_{20}Te_{18}(PEt_3)_{12}$ (ethyl groups were omitted for clarity). Reprinted with permission from [66]. Copyright 1989 American Chemical Society.

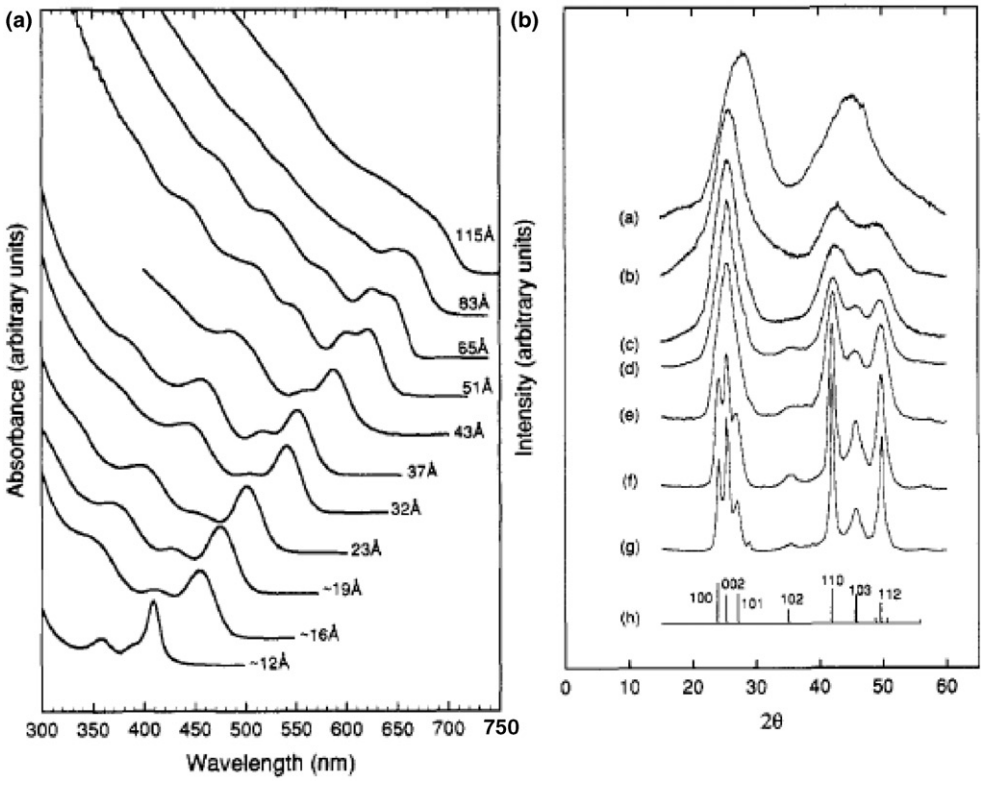

Figure 7. (A) CdSe absorption spectra for diameters ranging between 1.2 and 11.5 nm. (B) Powder XRD spectra for CdSe nanocrystals with diameters of: (a) 1.2 nm, (b) 1.8 nm, (c) 2.0 nm, (d) 3.7 nm, (e) 4.2 nm, (f) 8.3 nm and (g) 11.5 nm. Reprinted with permission from [77]. Copyright 1993 American Chemical Society.

high boiling points and can datively bind to metal complexes) [74–76]. Sizes based upon the Scherrer formula underestimated diameters significantly and the authors contend that each nanocrystal might actually encompass two to four distinct crystal domains without any coherence between them. Annealing significantly narrowed XRD peaks, indicative of domain growth to very nearly the sizes observed by TEM rather than undertake pyrolysis *in vacuo*.

This annealing procedure motivated Murray *et al.* to develop a novel synthesis of nanocrystals [77]. The authors cite the work of Steigerwald and co-workers "on the use of organometallic precursors in the solution-phase synthesis of bulk and nanocrystalline materials" as guidance in their selection of reagents [42, 65, 78]. Dimethyl cadmium was utilized as the cation source while tertiary phosphine chalcogenides (Ch=Se and Te) and bis(TMS)Ch (Ch=S) sources were chosen as the anion precursors based on their ease of preparation and stabilities. After combining anion and cation sources in a nitrogen-filled glovebox, they were rapidly injected into a degassed melt of trioctylphosphine oxide (TOPO) at 300°C. Nucleation of CdCh was immediately evident by the appearance of a bright-yellow color. Fractions were removed at intervals during heating, which demonstrated that the absorption spectra continuously red-shifted over a period of several hours as the nanocrystals grew in diameter (figure 7a). This synthesis

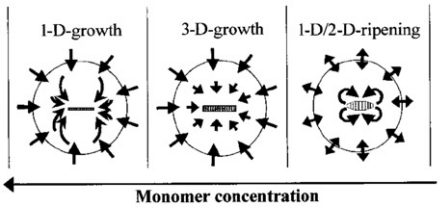

Figure 8. The shape of the growing nanocrystal changes as the monomer concentration increases from right to left in this schematic. The circle marks where the diffusion sphere meets the bulk solution. The single-sided arrows show the direction of the diffusion gradient of the monomers. Double-sided arrows indicate diffusion equilibrium. Reprinted with permission from [88]. Copyright 2001 American Chemical Society.

was able to produce nanocrystal sizes between 1.2 and 11.5 nm by controlling reaction temperatures and time. XRD patterns for different-sized nanocrystals are shown in figure 7(b). The dependence of crystallite size on linewidths is clearly demonstrated and consistent with the predicted broadening based upon the Scherrer equation for sizes determined by TEM measurements. Size-distributions measured by TEM are less than 10% but can reach 5% by using size-selective precipitation.

As a demonstration of this method's capability, Murray *et al*. later showed that nanocrystals can self-organize spontaneously into three-dimensional superlattices [79]. This degree of organization necessitates near uniformity of size and shape. They even showed that interparticle packing was directly controlled by the length of the surface ligand using small angle XRD. This result further develops the image of the nanocrystal as an inorganic core surrounded by surfactant-like molecules, both electronically passivating surface atoms and surrounding the nanocrystal in a colloid-like shell.

The improved size dispersities from the Murray method resulted in extremely resolved optical spectra. Absorption and emission linewidths were significantly narrower than had previously been observed. Without the large polydispersity of nanocrystal sizes, which resulted in peak overlaps that obscured optical spectra, researchers were able to assign higher-order electronic transitions in CdSe nanocrystals; five excitonic transitions, in addition to the often-observed lowest energy transition, were now resolvable [80]. In addition, new photophysical phenomena were observed in nanocrystals, such as single-particle PL blinking [81, 82]. Also, new applications such as bio-labeling [83, 84], light-emitting diodes [85] and lasers [86] were made possible.

4.3. *Batch-to-batch reproducibility in size and shape control with the TOPO synthesis*

The paper that marked the beginning of the modern era of QD research was the first major contribution to methodology for controlling the shape of nanocrystals. Peng and coworkers determined that, when nanocrystal growth rates are fast, growth along the *c* (most polar) axis of the wurtzite crystal of CdSe is favored, consequently rod-shaped nanocrystals form. They achieved their goal of producing rods that were monodisperse in shape and size by improving the control of the growth kinetics. The authors found that the growth along the faces of the nanocrystals became slower when they added varying amounts of hexylphosphonic acid. Syntheses performed with technical grade TOPO exhibit faster nanocrystal growth than those done using pure TOPO, but the authors did not want their results to be dependent on the presence of impurities. As an

alternative, they chose to dope pure TOPO with a ligand that binds more strongly to cadmium than does TOPO [87]. A year later Peng and coworkers provided more strategies for forming anisotropic nanocrystals. They suggested that the growth reaction is, under certain conditions, diffusion controlled: for example, the longer the length of the alkyl chain of the cadmium monomer, the lower the diffusion coefficient of the precursor, and the slower the growth of the rods overall. Slow growth can, however, favor anisotropic growth because the crystal planes perpendicular to the *c*-axis have the highest reactivity. The concentration gradient, and therefore the flux, of the cadmium monomer are highest in the proximity of these planes, and these local gradients drive 1-D growth of the rods (see figure 8 for a schematic representation of these growth mechanisms). The presence of these diffusion gradients depends on the presence of a minimum amount of cadmium monomer, so the mechanism is not only controlled by the chemistry of the cadmium precursor, but also its concentration [88]. The TEM images in figure 9 depict how the shape of the nanocrystal changes with monomer concentration.

4.4. *The trouble with TOPO [89]*

The first report to examine explicitly the irreproducibility of the TOPO/TOP synthesis for cadmium chalcogenide QDs appeared in 2008. Wang *et al*. identified a set of impurities in reagent grade (90%) TOPO, shown in figure 10, and compared the product formed with 90% TOPO to that formed with distilled 99% TOPO controllably

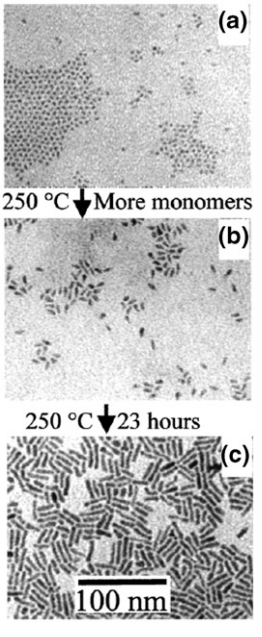

Figure 9. TEM images demonstrating growth of quantum rods from quantum dots upon addition of more precursors. This precursor addition provides a higher monomer concentration to facilitate rod growth. Reprinted with permission from [88]. Copyright 2001 American Chemical Society.

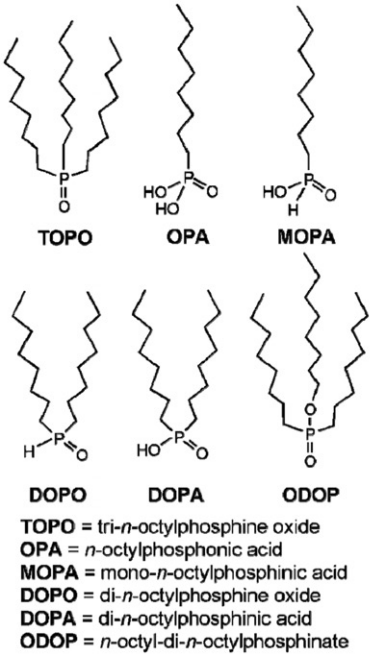

Figure 10. The contents of tech grade TOPO and their corresponding chemical structures. Reprinted with permission from [89]. Copyright 2008 American Chemical Society.

doped with each impurity [89]. This article reports that the addition of the impurities di-*n*-octylphosphonic acid (DOPA) and di-*n*-octylphosphine oxide (DOPO) resulted in QDs with lower shape and size dispersities as well as higher crystallinity. Further NMR studies by Kopping *et al*. showed that the impurities in TOPO, particularly octylphosphonic acid (OPA) and *P*′-*P*′-(di-*n*-octyl)dihydrogen pyrophosphonic acid, the self-condensation product of OPA, make up a dominant fraction of the ligands on the QD surface post-synthesis; the majority ingredients in the synthesis – TOPO, hexadecylamine (HDA), TOP, and TOPSe – were present on the surface in very low concentrations [90].

Morris-Cohen *et al*. demonstrated that the presence of OPA in the reaction mixture results in CdSe QDs with surfaces that are significantly enriched in cadmium [91]. This enrichment is amplified as the QDs get smaller and is driven by the presence of negatively charged alkylphosphonates in the reaction mixture. Alkylphosphonates outcompete weaker-binding ligands like TOPO, TOP, HDA, and TOPSe, and are, in fact, the only ligands present on the QDs after successive precipitations from MeOH (the most common non-solvent used for purification of the QDs) [91]. The absence of alkylphosphonates in the synthetic mixture leads to QDs with ~1 : 1 ratio of Cd : Se, but with poorer size dispersity and quality.

Advancements in surface characterization methods facilitated the analysis of the role of reagent impurities in the final chemical composition of QDs. NMR [90–93] and FT-IR [94, 95] are the most commonly-used techniques for identifying ligands on the surfaces of QDs, monitoring the progress of a ligand exchange, and determining how certain ligands bind to the surface [93]. NMR is also useful for studying the equilibrium

between the ligands that are bound to the QD surface and the ligands that are free in the solution. Bound ligands produce peaks that are broader than those produced by free ligand [96], and diffusion times from diffusion ordered spectroscopy spectra and cross-peaks from nuclear the Overhauser effect spectroscopy (NOESY) spectra reveal whether the ligand interacts with other ligands on the surface of the QD [97]. This differentiation between signals from bound and free ligands led to the use of ^{1}H-NMR and NOESY NMR to calculate ligand binding constants [98].

Inductively-coupled plasma atomic emission spectroscopy (ICP-AES) and mass spectrometry (ICP-MS) have been used to quantitavely estimate the surface ligand coverage [91, 99] and determine the elemental composition of the QD core and shell [91, 99, 100]. ICP techniques are primarily only useful for metals and semi-metals due to the fact that the plasma does not efficiently excite non-metallic elements. Sulfur and phosphorus are notable exceptions to this rule, but the use of ICP techniques to detect these elements is restricted by the relatively high limits of detection for these elements.

4.5. *A safer, greener, and more effective cadmium precursor*

Peng and coworkers also published landmark papers on syntheses employing TOPO as the coordinating solvent, but used alternative cadmium precursors to dimethylcadmium [101, 102]. They showed that these new precursors, such as cadmium complexed with tetradecylphosphonic acid, decreased the size dispersity to 15% or less, and increased the reproducibility of the synthesis. Qu *et al*. further demonstrated that the combination of CdO and a fatty acid imparted a similar effect on the reaction. These new cadmium precursors decompose more slowly than dimethylcadmium, so nucleation is slower and a higher monomer concentration persists during growth. The overall effect is that the growth of smaller particles is favored over that of larger particles, which results in a narrower size distribution (5–10%). Qu *et al*. tuned the diameter of CdSe QDs between 2 and 25 nm by changing the length of the fatty acid chain (see figure 11 for absorption spectra of these QDs), and they changed the crystal structure from wurtzite to zinc blende by adding alkylamines to the reaction mixture [101].

Yu and Peng further increased the size-tunability of cadmium chalcogenide QD by using seemingly uncoordinating solvents [103]. A report in 2008 would show that the assumption that these solvents do not coordinate to cadmium is not true [89]. Because these solvent molecules themselves do not stabilize the precursor ions, they enabled greater control over the ratios of coordinating ligand to other precursors; these ratios are important to control because they have a large impact on the size dispersity of the QDs. This advancement not only resulted in more synthetic control of size and dispersity, but also expanded the number of solvents that could be used for QD syntheses. Yu and Peng highlighted the use of the ''non-coordinating'' solvent octadecene, which is also an effective reducing agent for the elemental sulfur precursor [103].

4.6. *Work toward enhancement of PL intensity*

In 2002, Peng and coworkers focused on controlling the PL-QY of QDs. They achieved a PL-QY of 85% using a combination of CdO in stearic acid as the cadmium precursor, a mixture of TOPO and HDA as the coordinating solvent, and a 1 : 7 molar ratio of TBP selenide to dioctylamine as the selenium precursor. The authors credit the addition

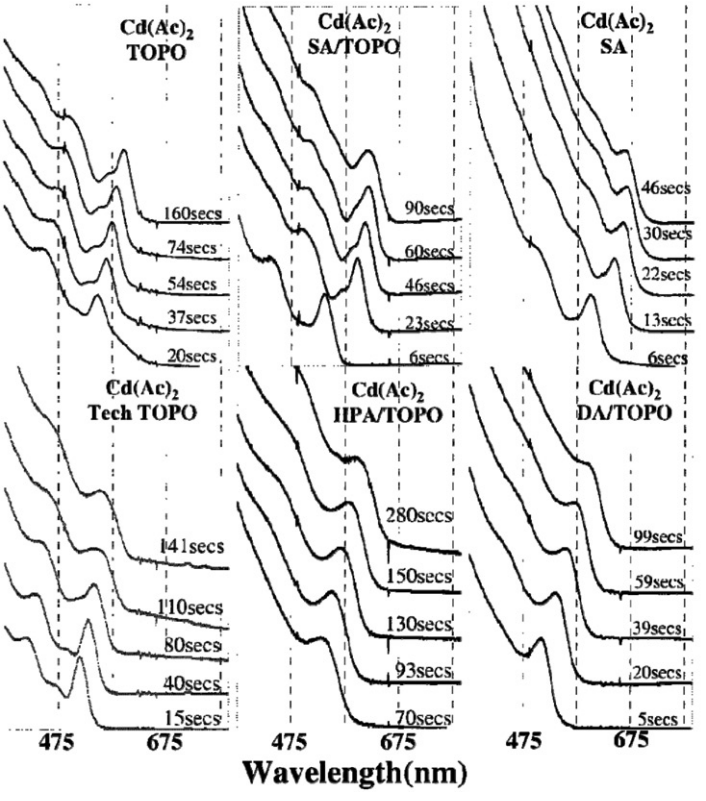

Figure 11. Absorption spectra taken at varying growth times of CdS QDs synthesized using different phosphonic and fatty acids. The reaction conditions for each of these syntheses was identical with the exceptions that the growth temperature for the reactions using DA/TOPO was lower, and that the reaction using HPA/TOPO used 0.66 mol HPA kg^{-1} of TOPO while the other two-component reaction solvents used equal amounts of each component. Reprinted with permission from [92]. Copyright 2001 American Chemical Society.

of the primary amine, HDA, with the exceptional passivation of the QD surfaces [104]. Similarly, in 1986, McLendon *et al.* had found that the post-synthesis addition of primary amines increased the PL-QY of their nanocrystals by up to 450%; amines are effective electron donors for incompletely coordinated cadmium ions that otherwise serve as electron traps and quench PL [23]. Talapin and coworkers published similar results in 2001 showing that nanocrystals of all shapes exhibited higher PL-QYs after ligand exchange with alkylamines [105]. In 2006, Bullen *et al.* reported a systematic study confirming that amines passivate *via* electron donation to incompletely coordinated Cd^{2+}, and that more sterically hindered alkylamines (namely, secondary and tertiary amines) achieved lower surface coverage, and therefore poorer surface passivation than straight-chain primary amines [106].

4.7. *Synthesis of lead chalcogenide QDs*

Many of the synthetic developments, such as the use of long-chain fatty acids and organometallic chalcogenide precursors, that improved the size and shape control of

cadmium chalcogenide QDs also enabled the synthesis of highly crystalline, monodisperse lead chalcogenide QDs. Murray and coworkers were the first to use these techniques to synthesize PbSe QDs [107]. They combined the precursors TOPSe and lead oleate in diphenyl ether and varied the growth temperature between 90°C and 220°C in order to tune the diameter of the QDs between 3.5 and 15 nm. The size dispersity of these QDs was 10%, but size-selective precipitation reduced this value to 5%. Murray was able to use lower temperatures than those applied in previous methods – and therefore produce smaller diameters than had been synthesized previously – by using less stable precursors. Several groups developed variations of Murray's synthesis to decrease size dispersity, improve PL-QY, and make PbSe/PbS core-shell QDs [108–110]. NMR and ICP-MS studies show that PbSe QDs grown using lead oleate as a precursor are lead-enriched, and that the surface of these QDs is passivated by a monolayer of Pb^{2+}-oleate complexes, with $<5\%$ of the ligand composition being TOP [92].

The first high-quality, colloidal PbS QD syntheses by Hines *et al.* [111] and Joo *et al.* [112] also incorporated long-chain coordinating ligands. Hines and Scholes used lead oleate as the Pb precursor and bis(trimethylsilyl)sulfide (TMS-sulfide) in octadecene as the sulfur precursor. By tuning the temperature between 80°C and 140°C, the authors obtained QDs with band-edge absorptions over a large range: 800–1800 nm with a standard deviation in the size of 10–15% [111]. Joo and coworkers used a reaction mixture of $PbCl_2$, elemental sulfur, and oleylamine, where the oleylamine served as both a ligand and the solvent. They used the Pb : S ratio, rather than reaction temperature, to tune the size; a smaller ratio led to larger nanocrystals. They observed, however, that, as the size changed, so did the morphology: smaller nanocrystals were spherical and larger nanocrystals were cubic [112]. Cademartiri *et al.* developed a variation on the $PbCl_2$, sulfur, and oleylamine synthesis in which the QDs grew at a much lower temperature, 100°C. They also used more $PbCl_2$ and less oleylamine to increase the viscosity of the solution, and thus the diffusion rate of the precursors was varied to control the reaction rate. However, they were also changing the absolute monomer concentration in the synthesis. Additionally, they found that the addition of primary amines to the reaction mixture inhibited the formation of cubic crystals [113]. In 2011, Moreels and coworkers reported that the addition of TOP to the sulfur/oleylamine precursor mixture increases the maximum achievable diameter of PbS QDs to 10 nm due to a strong interaction between sulfur and TOP that decreases the average reactivity of the sulfur precursor, and leads to the formation of fewer nuclei and therefore larger QDs on average [114].

The use of long alkyl chains in ligands and solvents in the synthesis of lead chalcogenide QDs introduced alkyl chain length as a variable to control size and shape. Lifshitz *et al.* reported that, when solvents with a longer alkyl-chain length are used, higher temperatures are required for nanocrystals to transition from wires to rods or multipods or from wires to dots then to cubes because the alkyl chain presents an energetic barrier for aggregation of the nanocrystals, which is required to form the branched shapes. Aggregation not only increases the average size, but also the size dispersity of the nanocrystals [115]. Baek *et al.* used a mixture of hexanoic acid and acetic acid in different ratios to control the size of PbSe QDs. Greater amounts of acetic acid, and therefore less steric repulsion between growing particles, led to the formation of larger, more crystalline QDs [116].

4.8. *Mechanisms of QD formation*

Classic work by LaMer and Dinegar proposed a growth model of monodisperse lyophobic colloids that accurately predicted their size-evolution simply based upon the concentration of monomers in the solution [117]. This model has since been applied to describe the formation of semiconductor nanocrystals [77] and metal nanoparticles [118]; yet, uncertainty remains regarding the mechanism of monomer formation and even the identity of the monomeric species in QD syntheses. Very limited work has been published concerning the reaction mechanism: two independent studies both concluded that reactions between tertiary phosphine chalcogenides (e.g., TOPSe) and metal carboxylates were the result of a Lewis acid–base complex [119, 120].

Alternatively, Krauss and co-workers identified that impurity quantities of secondary phosphine chalcogenides might account for all the observed reactivity since they are significantly more reactive with metal carboxylates than tertiary phosphine sources [121]. In that study, it was proposed that the acidic proton of the secondary phosphine chalcogenide initiated ligand disproportionation on the metal center *via* an acid–base exchange reaction producing an M–Ch bond and free carboxylic acid. The authors suggest that R′COO–M–Ch–PR_2 represents the structure of a potential monomer unit whereby intermolecular reactions between multiple monomers enlarges the cluster size but preserves the coordination chemistry of the monomer unit (i.e., carboxylate ligands on metals and phosphite ligands on the chalcogenide). These authors contend that a parallel can be drawn between this chemistry and condensation polymerization, which highlights earlier contentions that regarded QDs as inorganic living polymers [42].

It should be noted that other chemical pathways may exist that the authors of the prior studies have not addressed. For instance, metal carboxylates are known to decarboxylate and generate metal-alkyl species [122]. Copper carboxylates have been shown to decarboxylate at temperatures as low as 60°C [123]. This result would be ironic when considering that metal carboxylates were first employed to avoid the use of metal alkyls. Nonetheless, a better understanding of chemical mechanism is anticipated to enable future improvements in synthetic conditions, QD structure (shape/size/surface), and perhaps even facilitate the use of new precursors.

4.9. *Inorganic ligands*

Analogous to the advantageous effects of switching from ionic to organometallic synthetic precursors, transitioning from organic to inorganic capping ligands has had similar effects on electron mobilities of QD-based materials. Early attempts at improving the electron mobility of QD-based materials focused on reducing inter-particle spacing while maintaining electronic passivation of the QD surface. Kuno *et al*. found that the removal of long-chain, insulating ligands introduced charge traps and produced poorly-passivated QD surfaces [124]. A few years later Yu *et al*. used 1,4-phenylenediamine as a short-chain capping ligand to improve electron mobility, which was effective at passivating the QD surface but the QDs were not reliably stable [125]. The inability to achieve a balance between small interparticle spacing and effective surface passivation motivated the recent post-synthetic modifications of capping chemistry by Talapin and co-workers. In 2009, Kovalenko *et al*. exchanged the insulating organic ligands of the QDs for inorganic ligands by immersing QDs in an organic solution of tin chalcogenides in hydrazine at elevated temperatures [126]. In 2010, the same group performed this

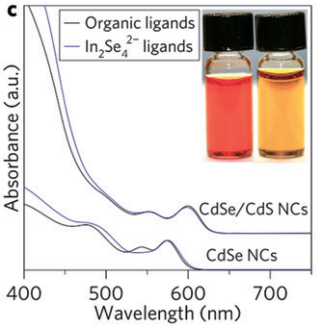

Figure 12. Absorption spectra of CdSe and CdSe/CdS nanocrystals capped with organic (black) and inorganic, $In_2Se_4^{2-}$, (blue) ligands. The sample with inorganic ligands exhibited slightly higher absorbance at short wavelengths but had little effect on the band-edge absorbances of the QDs. The inset shows photographs of these solutions capped with $In_2Se_4^{2-}$. Reprinted by permission from Macmillan Publishers Ltd: Nature Nanotechnology, [113], copyright 2011.

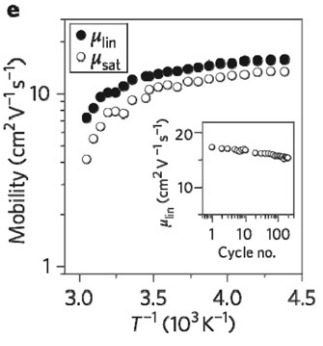

Figure 13. Field-effect mobility as a function of temperature for an n-channel field-effect transistor comprised of 3.9 nm CdSe QDs capped with $In_2Se_4^{2-}$. The inset shows how this mobility changes as the gate voltage is cycled between −30 V and +30 V 200 times with the drain-source voltage set at 2 V. Reprinted by permission from Macmillan Publishers Ltd: Nature Nanotechnology, [113], copyright 2011.

exchange with a variety of tin, arsenic, and molybdenum chalcogenide ligands, and found that more environmentally friendly solvents, formamide, water, and dimethylsulfoxide, could be substituted for hydrazine. Field-effect transistors comprising these new, all-inorganic QDs as the channel material displayed electron mobilities of $1.4 \times 10^{-5}\,cm^2\,V^{-1}s^{-1}$ [127]. Researchers in the Talapin group continued to work on this inorganic ligand strategy. Lee *et al.* observed an electron mobility of $16\,cm^2\,V^{-1}s^{-1}$ in films of QDs functionalized with $In_2Se_4^{2-}$ [128]. Figures 12 and 13 show the absorption spectra and electron mobility data for these QDs, respectively. This value is the highest observed electron mobility for QD-based materials.

5. Conclusions

The impressive advancements in the tunability of QD size, morphology, and crystal structure as well as the increased understanding of QD growth mechanisms and

implementation of novel ligands that we have described here have greatly improved the optical and electronic properties of QDs. QD-based photovoltaics have benefited from improved stability of QDs in air, especially in the case of lead-chalcogenide QDs. The efficiencies of PbS photovoltaic devices are approaching that of polymer devices, and have shown the potential to exploit carrier multiplication (multiple carriers per incoming photon). Poor transport of charge carriers under the low-bias conditions of a solar cell is still limiting the performance of QD-based devices. Current efforts focus on improving the performance by using nanorods for directional charge transport, incorporation of QDs into the bulk heterojunction architecture (which has been the most successful morphology for all-organic cells), and the use of nanoporous electrodes [129]. Further improvement in surface passivation of the QDs with minimal interparticle spacing (perhaps through Talapin's inorganic ligand strategy) will certainly be a major ingredient in producing films with higher carrier mobilities, and the use of core-shell architectures is a promising strategy for optimizing the thermal stability of these devices.

The application of QDs to imaging of biomolecules has progressed more quickly than has their application in energy conversion. Water-soluble cadmium chalogenide QDs have been integrated into QD-antibody and QD-peptide conjugates, and tested *in vivo* and *in vitro* for imaging of prostate, breast, pancreatic, liver, and tongue cancers. While these QD-based materials are successful in targeting and imaging cancer cells, improvements in target specificity, signal intensity, and therapeutic efficacy, and more knowledge of QD toxicity and pharmacology are needed in order to advance further [130]. Surface chemistry, in the form of robust protective organic layers that quantitatively prevent leakage of metal ions into the surrounding medium, will continue to play a major role in exploiting the unique properties of semiconductor nanocrystals in biology, as it will in producing efficient QD-based energy conversion devices.

Acknowledgments

The authors acknowledge the support of the Army Research Office *via* the Presidential Early Career Award for Scientists and Engineers (PECASE) to EAW, and the IGERT: Quantum Coherent Optical and Matter Systems Program (NSF Award number 0801685).

References

[1] C.B. Murray, C.R. Kagan, M.G. Bawendi. *Ann. Rev. Mater. Sci.*, **30**, 545 (2000).
[2] K. Kalyanasundaram, E. Borgarello, D. Duonghong, M. Gratzel. *Angew. Chem. Int. Ed. Engl.*, **20**, 987 (1981).
[3] A.J. Nozik. *Ann. Rev. Phys. Chem.*, **29**, 189 (1978).
[4] A. Fujishima, K. Honda. *Nature*, **238**, 37 (1972).
[5] R. Williams. *J. Chem. Phys.*, **32**, 1505 (1960).
[6] B. O'Regan, M. Gratzel. *Nature*, **353**, 737 (1991).
[7] R. Rossetti, J.L. Ellison, J.M. Gibson, L.E. Brus. *J. Chem. Phys.*, **80**, 4464 (1984).
[8] A.Y. Cho, J.R. Arthur. *Prog. Solid-State Chem.*, **10**, 157 (1975).
[9] P.A. Kohl, S.N. Frank, A.J. Bard. *J. Electrochem. Soc.*, **124**, 225 (1977).
[10] A. Henglein. *J. Phys. Chem.*, **86**, 2291 (1982).

[11] A. Henglein. *Ber. Bunsenges. Phys. Chem.*, **86**, 301 (1982).
[12] A. Fojtik, H. Weller, U. Koch, A. Henglein. *Ber. Bunsenges. Phys. Chem.*, **88**, 969 (1984).
[13] H. Weller, U. Koch, M. Gutierrez, A. Henglein. *Ber. Bunsenges. Phys. Chem.*, **88**, 649 (1984).
[14] R. Rossetti, L.E. Brus. *J. Phys. Chem.*, **86**, 4470 (1982).
[15] R. Rossetti, S. Nakahara, L.E. Brus. *J. Chem. Phys.*, **79**, 1086 (1983).
[16] R. Dingle, W. Weigmann, C.H. Henry. *Phys. Rev. Lett.*, **33**, 827 (1974).
[17] R.C. Miller, D.A. Kleinman, W.T. Tsang, A.C. Gossard. *Phys. Rev. B*, **24**, 1134 (1981).
[18] L.E. Brus. *J. Chem. Phys.*, **80**, 4403 (1984).
[19] R. Rossetti, R. Hull, J.M. Gibson, L.E. Brus. *J. Chem. Phys.*, **82**, 552 (1985).
[20] J.J. Ramsden, M. Gratzel. *J. Chem. Soc., Faraday Trans.*, **80**, 919 (1984).
[21] M. Kundu, A.A. Khosravi, S.K. Kulkarni. *J. Mater. Sci.*, **32**, 245 (1997).
[22] A.J. Nozik, F. Williams, M.T. Nenadovic, T. Rajh, O.I. Micic. *J. Phys. Chem.*, **89**, 397 (1985).
[23] T. Dannhauser, M. O'Neil, K. Johansson, D. Whitten, G. McLendon. *J. Phys. Chem.*, **90**, 6074 (1986).
[24] N. Chestnoy, R. Hull, L.E. Brus. *J. Chem. Phys.*, **85**, 2237 (1986).
[25] L.E. Brus. *J. Phys. Chem.*, **90**, 2555 (1986).
[26] J.H. Fendler. *Chem. Rev.*, **87**, 877 (1987).
[27] P.L. Luisi, M. Giomini, M.P. Pileni, B.H. Robinson. *Biochim. Biophys. Acta*, **947**, 209 (1988).
[28] M. Gobe, K. Kon-No, K. Kandori, A. Kitahara. *J. Colloid Interface Sci.*, **93**, 293 (1983).
[29] S. Mann, A.J. Skarnulis, R.J.P. Williams. *J. Chem. Soc., Chem. Commun.*, 1067 (1979).
[30] M. Boutonnet, J. Kizling, P. Stenius, G. Maire. *Colloids Surf.*, **5**, 209 (1982).
[31] M. Faraday. *Philos. Trans. R. Soc. London*, **147**, 145 (1857).
[32] J. Turkevich, P.C. Stevenson, J. Hillier. *Discuss. Faraday Soc.*, **11**, 21 (1951).
[33] M. Meyer, C. Wallberg, K. Kurihara, J.H. Fendler. *J. Chem. Soc., Chem. Commun.*, 90 (1984).
[34] P. Lianos, J.K. Thomas. *Chem. Phys. Lett.*, **125**, 299 (1986).
[35] H.J. Watzke, J.H. Fendler. *J. Phys. Chem.*, **91**, 854 (1987).
[36] Y. Wang, N. Herron. *J. Phys. Chem.*, **91**, 257 (1987).
[37] K.K.W. Wong, S. Mann. *Adv. Mater. (Weinheim, Germany)*, **8**, 928 (1996).
[38] C.T. Dameron, R.N. Reese, R.K. Mehra, A.R. Kortan, P.J. Carroll, M.L. Steigerwald, L.E. Brus, D.R. Winge. *Nature*, **338**, 596 (1989).
[39] T. Klaus, R. Joerger, E. Olsson, C.-G. Granqvist. *Proc. Nat. Acad. Sci. USA*, **96**, 13611 (1999).
[40] J.N. Cha, K. Shimizu, Y. Zhou, S.C. Christiansen, B.F. Chmelka, G.D. Stucky, D.E. Morse. *Proc. Nat. Acad. Sci. USA*, **96**, 361 (1999).
[41] R.R. Naik, S.J. Stringer, G. Agarwal, S.E. Jones, M.O. Stone. *Nature Mater.*, **1**, 169 (2002).
[42] M.L. Steigerwald, A.P. Alivisatos, J.M. Gibson, T.D. Harris, R. Kortan, A.J. Muller, A.M. Thayer, T.M. Duncan, D.C. Douglass, L.E. Brus. *J. Am. Chem. Soc.*, **110**, 3046 (1988).
[43] A.R. Kortan, R. Hull, R.L. Opila, M.G. Bawendi, M.L. Steigerwald, P.J. Carroll, L.E. Brus. *J. Am. Chem. Soc.*, **112**, 1327 (1990).
[44] M.A. Marcus, W. Flood, M.L. Steigerwald, L.E. Brus, M.G. Bawendi. *J. Phys. Chem.*, **95**, 1572 (1991).
[45] A. Eychmuller, A. Mews, H. Weller. *Chem. Phys. Lett.*, **208**, 59 (1993).
[46] A. Mews, A. Eychmuller, M. Giersig, D. Schooss, H. Weller. *J. Phys. Chem.*, **98**, 934 (1994).
[47] A.P. Alivisatos, A.L. Harris, N.J. Levinos, M.L. Steigerwald, L.E. Brus. *J. Chem. Phys.*, **89**, 4001 (1988).
[48] V.L. Colvin, A.N. Goldstein, A.P. Alivisatos. *J. Am. Chem. Soc.*, **114**, 5221 (1992).
[49] N. Herron, Y. Wang, H. Eckert. *J. Am. Chem. Soc.*, **112**, 1322 (1990).
[50] A.N. Goldstein, C.M. Echer, A.P. Alivisatos. *Science*, **256**, 1425 (1992).
[51] Z. Alfassi, D. Bahnemann, A. Henglein. *J. Phys. Chem.*, **86**, 4656 (1982).
[52] M.A. Hines, P. Guyot-Sionnest. *J. Phys. Chem.*, **100**, 468 (1996).
[53] L.M. Liz-Marzan, M. Giersig, P. Mulvaney. *Langmuir*, **12**, 4329 (1996).
[54] K.E. Knowles, D.B. Tice, E.A. McArthur, G.C. Solomon, E.A. Weiss. *J. Am. Chem. Soc.*, **132**, 1041 (2010).
[55] M. O'Neil, J. Marohn, G. McLendon. *J. Phys. Chem.*, **94**, 4356 (1990).
[56] D. Fenske, J. Hachgenei, J. Ohmer. *Angew. Chem., Int. Ed. in English*, **24**, 706 (1985).
[57] D. Fenske, J. Ohmer, J. Hachgenei. *Angew. Chem., Int. Ed. in English*, **24**, 993 (1985).
[58] Y. Do, E.D. Simhon, R.H. Holm. *Inorg. Chem. (Washington, DC, United States)*, **24**, 2827 (1985).
[59] J. Sola, Y. Do, J.M. Berg, R.H. Holm. *Inorg. Chem. (Washington, DC, United States)*, **24**, 1706 (1985).
[60] S.J.C. Irvine, J. Giess, J.S. Gough, G.W. Blackmore, A. Royle, J.B. Mullin, N.G. Chew, A.G. Cullis. *J. Cryst. Growth*, **77**, 437 (1986).
[61] W.-W. Du Mont, H.-J. Kroth. *J. Organomet. Chem.*, **113**, C35 (1976).
[62] R.A. Zingaro, B.H. Steeves, K. Irgolic. *J. Organomet. Chem.*, **4**, 320 (1965).
[63] A. Darkowski, M. Cocivera. *J. Electrochem. Soc.*, **132**, 2768 (1985).
[64] M.L. Steigerwald, C.R. Sprinkle. *Organometallics*, **7**, 245 (1988).
[65] S.M. Stuczynski, J.G. Brennan, M.L. Steigerwald. *Inorg. Chem.*, **28**, 4431 (1989).
[66] J.G. Brennan, T. Siegrist, S.M. Stuczynski, M.L. Steigerwald. *J. Am. Chem. Soc.*, **111**, 9240 (1989).
[67] M.L. Steigerwald, C.E. Rice. *J. Am. Chem. Soc.*, **110**, 4228 (1988).
[68] M.L. Steigerwald. *Chem. Mater.*, **1**, 52 (1989).

[69] J.G. Brennan, T. Siegrist, S.M. Stuczynski, M.L. Steigerwald. *J. Am. Chem. Soc.*, **112**, 9233 (1990).
[70] M.L. Steigerwald, T. Siegrist, S.M. Stuczynski. *Inorg. Chem.*, **30**, 4940 (1991).
[71] S.M. Stuczynski, Y.-U. Kwon, M.L. Steigerwald. *J. Organomet. Chem.*, **449**, 167 (1993).
[72] M.L. Steigerwald, C.R. Sprinkle. *J. Am. Chem. Soc.*, **109**, 7200 (1987).
[73] J.G. Brennan, T. Siegrist, P.J. Carroll, S.M. Stuczynski, P. Reynders, L.E. Brus, M.L. Steigerwald. *Chem. Mater.*, **2**, 403 (1990).
[74] M.G. Bawendi, A.R. Kortan, M.L. Steigerwald, L.E. Brus. *J. Chem. Phys.*, **91**, 7282 (1989).
[75] M.G. Bawendi, W.L. Wilson, L. Rothberg, P.J. Carroll, T.M. Jedju, M.L. Steigerwald, L.E. Brus. *Phys. Rev. Lett.*, **65**, 1623 (1990).
[76] M.G. Bawendi, P.J. Carroll, W.L. Wilson, L.E. Brus. *J. Chem. Phys.*, **96**, 946 (1992).
[77] C.B. Murray, D.J. Norris, M.G. Bawendi. *J. Am. Chem. Soc.*, **115**, 8706 (1993).
[78] J.G. Brennan, T. Siegrist, P.J. Carroll, S.M. Stuczynski, L.E. Brus, M.L. Steigerwald. *J. Am. Chem. Soc.*, **111**, 4141 (1989).
[79] C.B. Murray, C.R. Kagan, M.G. Bawendi. *Science*, **270**, 1335 (1995).
[80] D.J. Norris, M.G. Bawendi. *Phys. Rev. B*, **53**, 16338 (1996).
[81] S.A. Blanton, A. Dehestani, P.C. Lin, P. Guyot-Sionnest. *Chem. Phys. Lett.*, **229**, 317 (1994).
[82] M. Nirmal, B.O. Dabbousi, M.G. Bawendi, J.J. Macklin, J.K. Trautman, T.D. Harris, L.E. Brus. *Nature*, **383**, 802 (1996).
[83] W.C.W. Chan, S. Nie. *Science*, **281**, 2016 (1998).
[84] M. Bruchez Jr., M. Moronne, P. Gin, S. Weiss, A.P. Alivisatos. *Science*, **281**, 2013 (1998).
[85] V.L. Colvin, M.C. Schlamp, A.P. Alivisatos. *Nature*, **370**, 354 (1994).
[86] V.I. Klimov, A.A. Mikhailovsky, S. Xu, A. Malko, J.A. Hollingsworth, C.A. Leatherdale, H.-J. Eisler, M.G. Bawendi. *Science*, **290**, 314 (2000).
[87] X. Peng, L. Manna, W. Yang, J. Wickham, E. Scher, A.V. Kadavanich, A.P. Alivisatos. *Nature*, **404**, 59 (2000).
[88] Z.A. Peng, X. Peng. *J. Am. Chem. Soc.*, **123**, 1389 (2001).
[89] F. Wang, R. Tang, W.E. Buhro. *Nano. Lett.*, **8**, 3521 (2008).
[90] J.T. Kopping, T.E. Patten. *J. Am. Chem. Soc.*, **130**, 5689 (2008).
[91] A.J. Morris-Cohen, M.D. Donakowski, K.E. Knowles, E.A. Weiss. *J. Phys. Chem. C*, **114**, 897 (2010).
[92] I. Moreels, K. Lambert, D. Smeets, D. De Muynck, T. Nollet, J.C. Martins, F. Vanhaecke, A. Vantomme, C. Delerue, G. Allan, Z. Hens. *ACS Nano*, **3**, 3023 (2009).
[93] R. Gomes, A. Hassinen, A. Szczygiel, Q.A. Zhao, A. Vantomme, J.C. Martins, Z. Hens. *J. Phys. Chem. Lett.*, **2**, 145 (2011).
[94] J.K. Cooper, A.M. Franco, S. Gul, C. Corrado, J.Z. Zhang. *Langmuir*, **27**, 8486 (2011).
[95] B. von Holt, S. Kudera, A. Weiss, T.E. Schrader, L. Manna, W.J. Parak, M. Braun. *J. Mater. Chem.*, **18**, 2728 (2008).
[96] I. Moreels, J.C. Martins, Z. Hens. *Chem. Phys. Chem.*, **7**, 1028 (2006).
[97] A. Hassinen, I. Moreels, C.D. Donega, J.C. Martins, Z. Hens. *J. Phys. Chem. Lett.*, **1**, 2577 (2010).
[98] M.D. Donakowski, J.M. Godbe, R. Sknepnek, K.E. Knowles, M.O. de la Cruz, E.A. Weiss. *J. Phys. Chem. C*, **114**, 22526 (2010).
[99] M.T. Frederick, E.A. Weiss. *ACS Nano*, **4**, 3195 (2010).
[100] A.R.M. Bustos, J.R. Encinar, M.T. Fernandez-Arguelles, J.M. Costa-Fernandez, A. Sanz-Medel. *Chem. Commun.*, 3107 (2009).
[101] L. Qu, Z.A. Peng, X. Peng. *Nano. Lett.*, **1**, 333 (2001).
[102] Z.A. Peng, X. Peng. *J. Am. Chem. Soc.*, **123**, 183 (2001).
[103] W.W. Yu, X. Peng. *Angew. Chem. Int. Ed.*, **41**, 2368 (2002).
[104] L. Qu, X. Peng. *J. Am. Chem. Soc.*, **124**, 2049 (2002).
[105] D.V. Talapin, A.L. Rogach, A. Kornowski, M. Haase, H. Weller. *Nature*, **1**, 207 (2001).
[106] C. Bullen, P. Mulvaney. *Langmuir*, **22**, 3007 (2006).
[107] C.B. Murray, S. Sun, W. Gaschler, H. Doyle, T.A. Betley, C.R. Kagan. *IBM Res. & Dev.*, **45**, 47 (2001).
[108] B.L. Wehrenberg, C. Wang, P. Guyot-Sionnest. *J. Phys. Chem. B*, **106**, 10634 (2002).
[109] A. Sashchiuk, L. Langof, R. Chaim, E. Lifshitz. *J. Cryst. Growth*, **240**, 431 (2002).
[110] H. Du, C. Chen, R. Krishnan, T.D. Krauss, J.M. Harbold, F.W. Wise, M.G. Thomas, J. Silcox. *Nano Lett.*, **2**, 1321 (2002).
[111] M.A. Hines, G.D. Scholes. *Adv. Mater.*, **15**, 1844 (2003).
[112] J. Joo, H.B. Na, T. Yu, J.H. Yu, Y.W. Kim, F. Wu, J.Z. Zhang, T. Hyeon. *J. Am. Chem. Soc.*, **125**, 11100 (2003).
[113] L. Cademartiri, J. Bertolotti, R. Sapienza, D.S. Wiersma, G. von Freymann, G.A. Ozin. *J. Phys. Chem. B*, **110**, 671 (2006).
[114] I. Moreels, Y. Justo, B. De Geyter, K. Haustraete, J.C. Martins, Z. Hens. *ACS Nano*, **5**, 2004 (2011).
[115] E. Lifshitz, M. Bashouti, V. Kloper, A. Kigel, M.S. Eisen, S. Berger. *Nano Lett.*, **3**, 857 (2003).
[116] I.C. Baek, S.I. Seok, N.C. Pramanik, S. Jana, M.A. Lim, B.Y. Ahn, C.J. Lee, Y.J. Jeong. *J. Coll. Inter. Sci.*, **310**, 163 (2007).
[117] V.K. LaMer, R.H. Dinegar. *J. Am. Chem. Soc.*, **72**, 4847 (1950).

[118] M. Brust, M. Walker, D. Bethell, D.J. Schiffrin, R. Whyman. *J. Chem. Soc., Chem. Commun.*, 801 (1994).
[119] J.S. Steckel, B.K.H. Yen, D.C. Oertel, M.G. Bawendi. *J. Am. Chem. Soc.*, **128**, 13032 (2006).
[120] H.T. Liu, J.S. Owen, A.P. Alivisatos. *J. Am. Chem. Soc.*, **129**, 305 (2007).
[121] C.M. Evans, M.E. Evans, T.D. Krauss. *J. Am. Chem. Soc.*, **132**, 10973 (2010).
[122] A.T.T. Hsieh, P.L. Sears, A.G. Lee. *J. Org. Chem.*, **37**, 2637 (1972).
[123] A. Cairncross, J.R. Roland, R.M. Henderson, W.A. Sheppard. *J. Am. Chem. Soc.*, **92**, 3187 (1970).
[124] M. Kuno, J.K. Lee, B.O. Dabbousi, F.V. Mikulec, M.G. Bawendi. *J. Chem. Phys.*, **106**, 9869 (1997).
[125] D. Yu, C. Wang, P. Guyot-Sionnest. *Science*, **300**, 1277 (2003).
[126] M.V. Kovalenko, M. Scheele, D.V. Talapin. *Science*, **324**, 1417 (2009).
[127] M.V. Kovalenko, M.I. Bodnarchuk, J. Zaumseil, J.-S. Lee, D.V. Talapin. *J. Am. Chem. Soc.*, **132**, 10085 (2010).
[128] J.-S. Lee, M.V. Kovalenko, J. Huang, D.S. Chung, D.V. Talapin. *Nat. Nanotechnol.*, **6**, 348 (2011).
[129] J. Tang, E.H. Sargent. *Adv. Mater.*, **23**, 12 (2011).
[130] V. Biju, S. Mundayoor, R.V. Omkumar, A. Anas, M. Ishikawa. *Biotech. Adv.*, **28**, 199 (2010).